Stratigraphic filtering and Q estimation

Gary F. Margrave

SUMMARY

The long-standing prediction that a seismic wave propagating in a finely layered earth model displays an apparent attenuation is investigated. Called stratigraphic filtering, this effect looks much like constant-Q attenuation and adds to intrinsic attenuation to produce effective attenuation. Using a 1D synthetic seismogram algorithm, this paper calculates the effective attenuation in a sequence of finely layered models derived from well logs. The models all have a finely-layered Q structure, representing intrinsic attenuation, derived from measured density and sonic logs by an empirical relation. The model properties are all sampled at 0.5 m intervals and averaged into constant thickness layers. Using 1m layers, when the Q value is carefully measured using the spectral-ratio technique, the measured Q is always lower than that expected from the specified model. In a series of experiments in which various physical effects are turned off and on again, it is demonstrated conclusively that this Q bias (measured Q - model Q) is due to internal multiples. Using a series of models derived from the same logs but with progressively thicker layers (each model has constant thickness layers and each is sampled a 0.5m) it is demonstrated that there is significant Q bias for layer thicknesses less than 20m but for thicknesses greater than this the Q bias disappears. The feasibility of estimating stratigraphic Q from such experiments and using these measurements to correct measurements form field data is discussed.

INTRODUCTION

The simulation of seismic waves in attenuating or anelastic media is a subject of considerable interest possibly because the earth is very strongly anelastic. Seismic wave recordings show strong frequency-dependent decay and this is usually understood as an indicator of anelastic behavior. (An excellent summary of current knowledge on this subject is found in Liner, 2012, Chapter 5.) Such decay contrasts with that from spherical divergence of wavefronts in 3D where the effect is not frequency dependent and is found for both elastic and anelastic waves. Conservation of energy requires that, while an elastic wave may appear to get weaker due to a variety of mechanisms, the total energy of the wave must remain constant. This is not the case for the anelastic wave because energy is converted from particle motion associated with waves to presumably heat within the material. Thus, any attempt experimentally to show energy conservation in the anelastic case would be expected to fail unless heat energy could be included.

Anelastic attenuation is usually parameterized with the value Q which is a dimensionless rock property defined as the ratio of wave energy to energy-loss per wave cycle. With this definition, large Q values indicate nearly elastic behavior where “large” is typically taken to mean greater than 200 (perfectly elastic materials have infinite Q). In contrast, Q values less than about 20 indicate highly lossy material such as might only be found in dry soil. The constant-Q theory (Kjartansson, 1979), which is used in this

paper, refers to a Q which is independent of frequency but still is allowed to vary arbitrarily with space. Very general causality arguments (Futterman, 1962) show that the exponential amplitude decay predicted by the constant-Q model must be accompanied by phase delays which are related mathematically to the amplitude attenuation. As a result, a wave propagating through an attenuating medium will become lower in overall amplitude, lower in frequency, and be delayed further in time, compared to the same wavelet propagating in a lossless medium.

O'Doherty and Anstey (1971, hereafter denoted ODA) presented an insightful analysis showing that waves propagating through a finely layered elastic medium show the same three effects just mentioned such that a finely layered elastic medium appears to be anelastic. This happens because the fine layering generates a complex train of interbred multiples that follow behind the primary wave front. The superposition of these multiples causes an exponential attenuation of higher frequencies that increases exponentially with traveltime. In a famous equation, they predicted that this exponential attenuation is determined by the autocorrelation of the reflectivity sequence that characterises the attenuation.

$$a(t,f) = e^{-\phi(f)t}$$

where $\phi(f)$ is the autocorrelation function. If the reflectivity is purely random, then $\phi(f)$ is independent of frequency and there is not stratigraphic filtering effect. However, when the reflectivity has a progressive trend, as it usually does, then $\phi(f)$ has a linear term that gives rise to an exponential attenuation that is similar to that from Q. Thus, they predicted that a propagating wave in a perfectly elastic, finely layered medium, will show a progressive loss of high frequency energy just as though the medium was actually anelastic.

The implications of ODA are profound and have been explored in many publications since then (Schoenberger and Levin, 1974, Richards and Menke 1983, Banik et al, 1985, Berlyand and Burridge, 1995). Presumably, a finely layered anelastic medium would then show two loss mechanisms: the intrinsic anelasticity of rocks and the stratigraphic filtering effect. This paper presents results from a numerical experiment demonstrating that this is indeed the case provided that the layering is sufficiently fine. The experiment uses a 1D synthetic seismogram algorithm originally presented by Ganley (1981) and described with extensions in Margrave and Daley (2014). This algorithm explicitly incorporates the constant Q model in each layer and has no limit on the number of layers or their thickness. It is found in the CREWES Matlab toolbox as *vspmodelq* for surface sources and *vspmodelqs* for buried sources (this paper used the former). Using velocity and density as measured in a well log, and a corresponding Q log built from an empirical relation between velocity, density, and Q (Margrave 2013), a synthetic VSP (vertical seismic profile) was created and subjected to Q measurements using the spectral-ratio method (Bath, 1974, see also Tonn, 1991, and Cheng, 2013). The resulting Q estimates are systematically lower, indicating more attenuation, than is expected from the Q log in the original earth model. Moreover, when a similar VSP was created using a modified

algorithm that turns off internal multiples, the Q measurements correspond precisely to those expected from the Q log. Comparing the two sets of Q measurements allows the estimation of the actual Q values arising from stratigraphic filtering alone. Thus separate estimates for intrinsic attenuation, Q_0, and stratigraphic attenuation, Q_{strat}, were obtained. Also, a perfectly elastic VSP, was constructed with the same velocity and density logs, and the resulting Q estimates correspond very well with the previously estimated Q_{strat}. All of these experiments were done with a model whose layers were 0.5 m thick and created as described from well measurements taken at 0.3048 m intervals. Then a series of similar experiments were created in which the log properties were blocked (Backus averaged) over progressively larger intervals while maintaining the same numerical depth sample size. It resulted that the stratigraphic filtering effect was progressively reduced as the well blocking increased and effectively vanished at a block size of about 20 m. This threshold blocking size is an estimate of how fine the layering must be to see the ODA effect and is about 10 times smaller than the dominant wavelength of the wavelet used in the experiment.

THE VSP MODELLING ALGORITHM

Here only an outline of the algorithm is presented while more detail and derivations can be found in Margrave and Daley (2014). The numerical computations were accomplished with a 1D visco-acoustic algorithm that includes all possible multiples and models attenuation using the constant-Q hypothesis of Kjartanssen (1979). That is, it is assumed that a wavelet propagates across the k^{th} homogeneous layer according to

$$\hat{w}(f) = \hat{w}_0(f) e^{-\pi f h_k/(Q_k v_k)} e^{-i2\pi f h_k/v_k} \tag{1}$$

where f is frequency, $\hat{w}_0(f)$ and $\hat{w}(f)$ are the initial and final Fourier transforms of the wavelet, and h_k, v_k, Q_k are the layer thickness, frequency-dependent phase velocity, and Q value respectively. The first exponential in this expression describes the frequency-dependent amplitude decay and the second exponential describes the frequency dependent delay with the velocity given by

$$v_k = \frac{v_0}{1 - \frac{1}{\pi Q_k}\ln\left(\frac{f}{f_0}\right)} \approx v_0\left[1 + \frac{1}{\pi Q_k}\ln\left(\frac{f}{f_0}\right)\right]. \tag{2}$$

Here v_0 is the velocity at the reference frequency, f_0, which is assumed to be the value measured in a sonic log which is typically done with f_0 near 12500 Hz. The frequency dependent time delays prescribed by equation 1 cause an initial impulse to evolve into a minimum phase wavelet.

Propagation from the deeper layer $k+1$ to layer k is described by

$$\begin{bmatrix} D_k \\ U_k \end{bmatrix} = \underline{\underline{A}}_k \begin{bmatrix} D_{k+1} \\ U_{k+1} \end{bmatrix} \tag{3}$$

where D_{k+1}, U_{k+1} are the downgoing and upgoing wavefields in the frequency domain at the top of layer $k+1$, D_k, U_k are similar wavefields at the top of layer k, and $\underline{\underline{A}}_k$ is the 2x2 layer matrix (sometimes called a propagator matrix) given by

$$\underline{\underline{A}}_k = \frac{1}{1-r_k} \begin{bmatrix} P_k^{-1} & Rr_k P_k^{-1} \\ Rr_k P_k & P_k \end{bmatrix} \tag{4}$$

in which r_k is the reflection coefficient for incidence from above on the interface between the layers, R takes the value -1 for a displacement solution and +1 for pressure, and $P_k = e^{-\pi f h_k/(Q_k v_k)} e^{-i2\pi f h_k/v_k}$ expresses the propagation across layer k. It follows from equation 3 that the fields in layer 1 and those in the bottom half space (layer $n+1$) can be related by

$$\begin{bmatrix} D_1 \\ U_1 \end{bmatrix} = \underline{\underline{A}} \begin{bmatrix} D_{n+1} \\ U_{n+1} \end{bmatrix} \tag{5}$$

where

$$\underline{\underline{A}} \equiv \prod_{k=1}^{n} \underline{\underline{A}}_k \,. \tag{6}$$

For a surface source, the VSP solution follows from equation 5 by setting the upgoing field in layer $n+1$ to zero and relating the up and downgoing fields in layer 1 through the free surface reflection coefficient. The result is

$$\begin{bmatrix} W - Rr_0 U_1 \\ U_1 \end{bmatrix} = \underline{\underline{A}} \begin{bmatrix} D_{n+1} \\ 0 \end{bmatrix}, \tag{7}$$

which is a 2x2 system of equations for the two unknowns U_1 and D_{n+1} and where W is the Fourier transform of the source waveform. The solution to equation 7 for all frequencies of interest determines the VSP wavefields. Once D_{n+1} is determined, the solution at any receiver can be determined from

$$\begin{bmatrix} D_r \\ U_r \end{bmatrix} = \underline{\underline{A}}_{r-n} \begin{bmatrix} D_{n+1} \\ 0 \end{bmatrix} \tag{8}$$

where r indicates the receiver layer and

$$\underline{\underline{A}}_{r-n} \equiv \prod_{k=r}^{n} \underline{\underline{A}}_k \,. \tag{9}$$

Equation 8 gives the solution at the top of layer r. Receivers inside the layer can be accommodated by phase shifting the solution at the layer top to the actual receiver position. See Margrave and Daley (2014) for more information. This algorithm is found in the CREWES Matlab toolbox as *vspmodelq*.

THE SPECTRAL RATIO METHOD OF Q ESTIMATION

Consider the experiment depicted in Figure 1 where a seismic source is positioned at the earth's surface near a vertical borehole. The source emits a waveform, $w_0(t)$, which is recorded at level (1) in the borehole and also at the deeper level (2). Using constant Q theory and neglecting wavefront spreading, the first arrival at level 1 can be modelled in the frequency domain as

$$\left|\hat{w}_1(f)\right| = \left|\hat{w}_0(f)\right| T_1 e^{-\pi f t_1/Q_1} \,. \tag{10}$$

Here $\left|\hat{w}_0(f)\right|$ and $\left|\hat{w}_1(f)\right|$ are the amplitude spectra emitted by the source and recorded at level (1) respectively, T_1 represents transmission effects between the source and level (1), t_1 is the traveltime, and Q_1 the average Q value between the source and level (1). In a similar fashion, the first arrival waveform at level (2) can be represented as

$$\left|\hat{w}_2(f)\right| = \left|\hat{w}_0(f)\right| T_2 e^{-\pi f t_2/Q_2} \,. \tag{11}$$

Now divide equation 11 by equation 10 and take the natural logarithm to form the *log spectral ratio*, or *lsr* , as

$$lsr(f) = \log \frac{\left|\hat{w}_2(f)\right|}{\left|\hat{w}_1(f)\right|} = \log\left(\frac{T_2}{T_1}\right) - \pi f \left(\frac{t_2}{Q_2} - \frac{t_1}{Q_1}\right). \tag{12}$$

Defining $T = T_2/T_1$, $\Delta t = t_2 - t_1$, and $Q_{\text{int}}^{-1} = \Delta t^{-1}\left(t_2/Q_2 - t_1/Q_1\right)$, equation 12 becomes

$$lsr(f) = \log(T) - \pi f \frac{\Delta t}{Q_{\text{int}}} \,. \tag{13}$$

Equation 13 predicts that a least-squares fit of a straight line to the *lsr* will have a slope of $m = -\pi f \Delta t/Q_{\text{int}}$ and an intercept of $b = \log(T)$. Since we expect $T_2 < T_1$ both slope and intercept normally should be negative values.

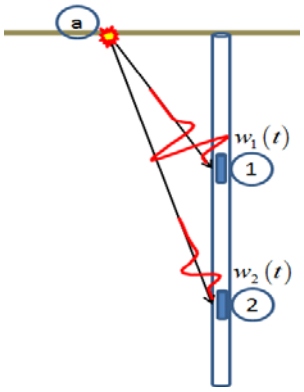

Figure `1: A Seismic source at (a) emits a wave that is recorded in a borehole at level 1 and a deeper level 2. The waveform recorded at level 1 is $w_1(t)$ while at level 2 it is $w_2(t)$.

As described, the spectral ratio method seems very straight forward but, in practice there difficulties. Most important is the choice of frequency band over which to do the least-square fit. In order to see the expected behaviour, the amplitude spectra of both $w_1(t)$ and $w_2(t)$ should significantly exceed noise levels over the range of the fit. A frequency range satisfying this criterion can be difficult to determine, especially for real data with high and variable noise. Even with synthetic data, the useful frequency range is limited by finite-precision computing which has a limited ability to model the strong exponential behaviour of Q attenuation. Figure 2 shows a typical spectral-ratio calculation for the data used in this study. Notice that the least-squares fit over 10-60 Hz give a very different linear estimate than a fit over 1-80 Hz. In this case, the 10-60 Hz estimate gives the correct result.

In the CREWES Matlab toolbox, there are currently three Q estimation methods to be found in the function *qestimator*, one of which is the spectral-ratio method used here. Also used in this paper is the tool *VSP_Q* which uses *qestimator* to make Q on a VSP.

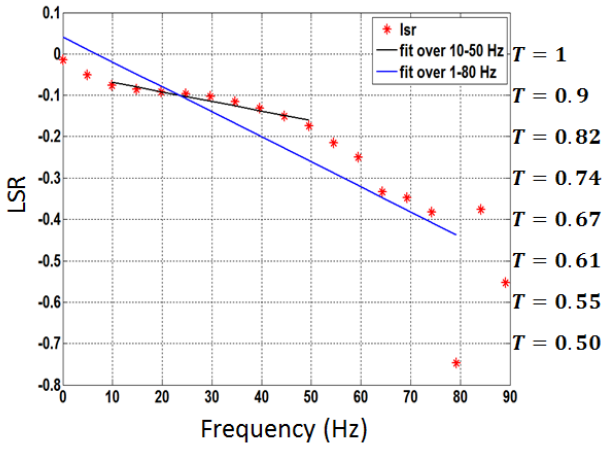

Figure 2: An illustration of a typical spectral ratio calculation as realized on the synthetic data of the algorithm described in this paper. A least-squares fit over the 10-50 Hz range gives an

approximately correct estimate for both Q and T which expanding the frequency range to 1-80 Hz leads to incorrect results as indicated by T greater than 1.0 .

THE WELL DATA AND THE MODEL USED

Figure 3 shows the well data used in this computation and the empirically derived Q model. The coloured curves in this figure show the data at the finest blocking size used in this study which is 0.5m. Blocking sizes up to 80m were used and the black dotted lines show the data as blocked as 20m as an example. Here "blocking" refers to averaging the velocity and density logs to produce logs with constant-values over the stated block size. All logs, regardless of blocking size were sampled at the same 0.5m interval. Thus, in the synthetic seismograms to come, all had the same number of layers even though, for a strongly blocked log, many of these layers had identical values. Since the maximum depth is about 1700m, there were about 3500 layers. Blocking was done using Backus averaging (Backus, 1962) and Q values were empirically derived from the blocked logs in each case.

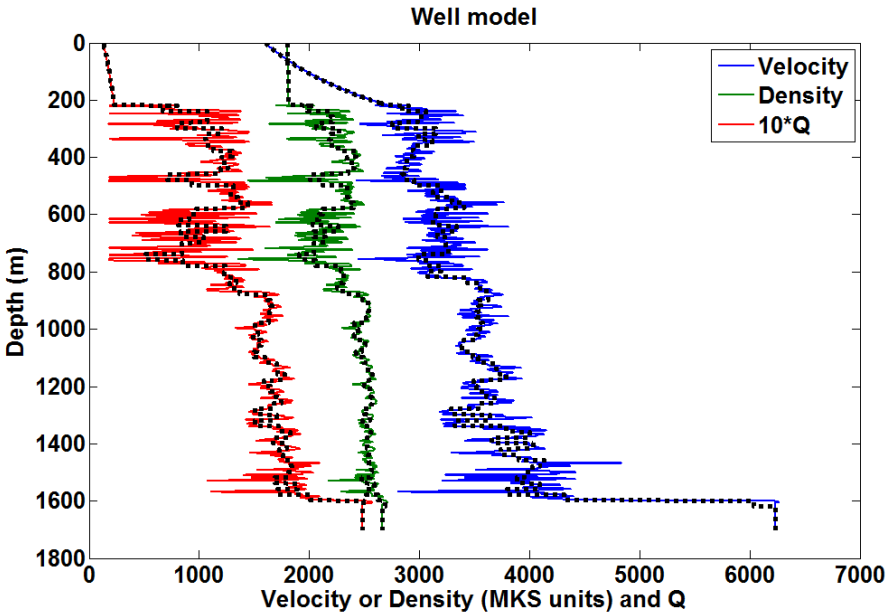

Figure 3: Velocity and density logs used in this study as well as the empirically derived profile. The coloured curves show the data at a blocking size of 0.5 m while the black dotted lines show the data as blocked at 20 m. The values are shown multiplied by 10 to allow them to plot easily on the same axis as the log data.

The empirical relation used to build the Q model calculates Q separately from the velocity and the density logs and then combines these. For the velocity log the estimate is

$$Q_v(z) = Q_0 \frac{v(z) - v_1}{v_0 - v_1} + Q_1 \frac{v(z) - v_0}{v_1 - v_0} \tag{14}$$

where Q_0, Q_1, v_0, v_1 are all constants and $v(z)$ represents the velocity log at some depth z. The form of equation 14 is such that when $v(z) = v_0$ then $Q_v(z) = Q_0$ and when $v(z) = v_1$ then $Q_v(z) = Q_1$. For any other velocity, the value is obtained from the linear relation defined by these four constant. In a similar fashion, the density relation is used to define

$$Q_\rho(z) = Q_0 \frac{\rho(z) - \rho_1}{\rho_0 - \rho_1} + Q_1 \frac{\rho(z) - \rho_0}{\rho_1 - \rho_0} \tag{15}$$

where ρ_0 and ρ_1 are constants and $\rho(z)$ represents the density log. The final Q model comes from combining these estimates according to

$$\frac{1}{Q(z)} = \frac{1}{Q_v(z)} + \frac{1}{Q_\rho(z)}. \tag{16}$$

Thus the final Q model combines the character of both velocity and density logs. The validity or utility of this Q model is not relevant to this study. The purpose here is simply to create a Q model with plausible fluctuations similar to those observed in the velocity and density logs.

Given a fine-structured Q model like that in Figure 3, it is necessary to ask what a spectral-ratio calculation can measure. In a VSP setting, the wavefield is first separated into upgoing and downgoing fields and Q estimates are made with the direct downgoing wave. The VSP modelling algorithm described previously produces perfectly separated upgoing and downgoing fields so the wavefield separation technique is not relevant here. Given the downgoing fields corresponding to receivers at depths z_1 and z_2, the amplitude spectra can be compared in a spectral ratio test. If $A_1(f)$ and $A_2(f)$ represent the amplitude spectra, then considering primary arrivals only (no multiples) these spectra will be related by

$$A_2(f) = A_1(f) \prod_k e^{-\pi f \Delta t_k / Q_k} \tag{17}$$

where the index k in the product ranges over all layers between z_1 and z_2 (I assume both depths are at layer tops for simplicity). This expression is equivalent to

$$A_2(f) = A_1(f) e^{-\pi f \sum_k \Delta t_k / Q_k}. \tag{18}$$

The spectral ratio method measures a single interval, Q_{int}, corresponding to the total attenuation effect between the receivers. Comparing equations 18 and 13 leads to the expectation

$$\frac{\Delta t}{Q_{\text{int}}} = \sum_k \Delta t_k / Q_k \tag{19}$$

where $\Delta t = t_2 - t_1$ in which t_1 and t_2 are first arrival times corresponding to depths z_1 and z_2. Thus the expected result from the spectral-ratio calculation is

$$Q_{\text{int}} = \frac{\Delta t}{\sum_k \Delta t_k / Q_k}. \tag{20}$$

This calculation is accomplished by the tool *qz2qint* in the CREWES Matlab toolbox.

MEASURING STRATIGRAPHIC FILTERING

Using the VSP modelling algorithm described previously, and the model of Figure 3, the resulting VSP wavefield is shown in Figure 4 and the upgoing field is in Figure 5 while the downgoing field is in Figure 6. The upgoing and downgoing fields are computed exactly and are not estimated by a wavefield separation technique. Also show on Figure 6 are traveltimes for the direct downgoing arrival as computed at the logging frequency (12500 Hz) and at the dominant seismic frequency (30 Hz). The frequency dependence of velocity is predicted by constant Q theory as described by equation 2. The VSP modelling algorithm has accurately computed this delay as can be appreciated from the enlargement shown in Figure 7.

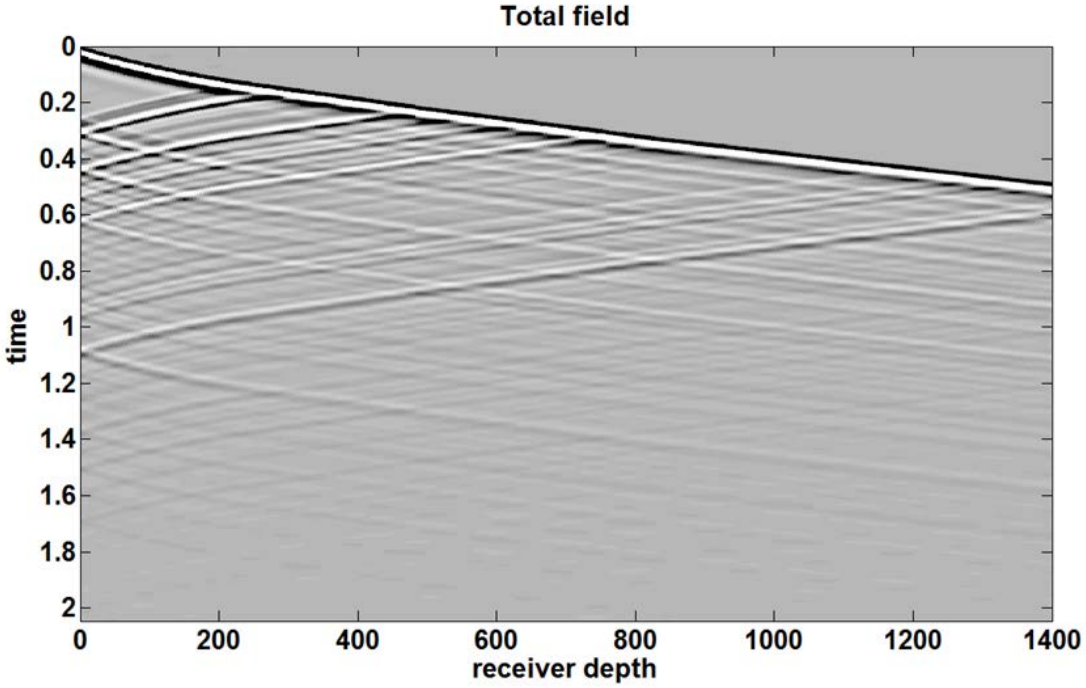

Figure 4: The total VSP wavefield corresponding to the finely sampled model (0.5 m blocking) of Figure 3.

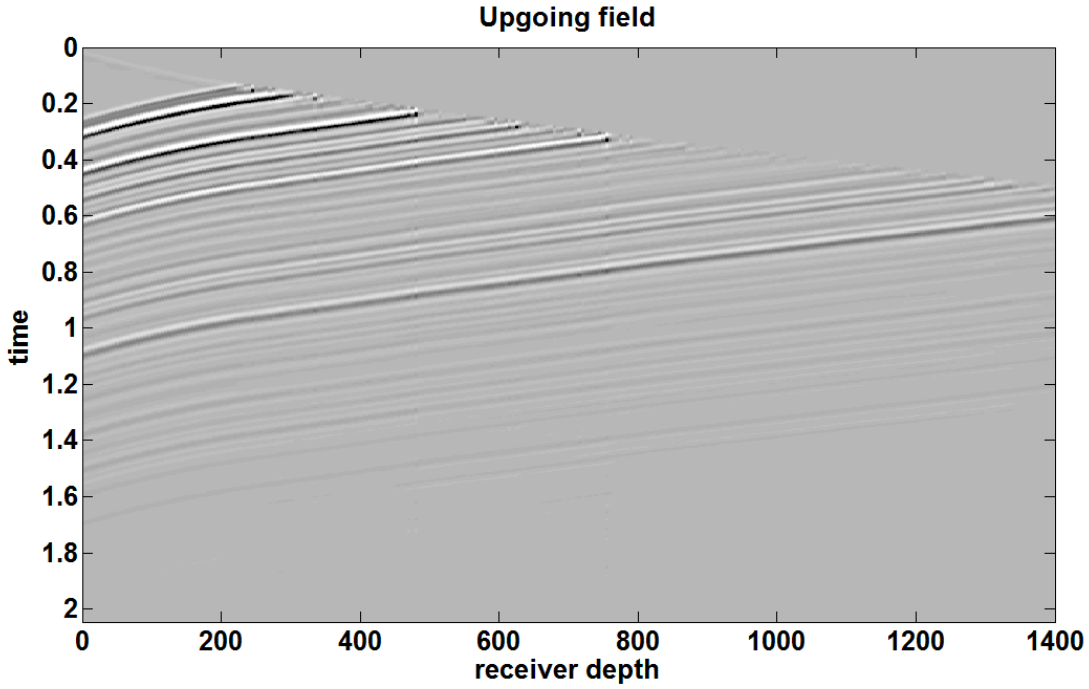

Figure 5: The upgoing wavefield from Figure 4. This is computed exactly by the modelling algorithm and is not estimated by wavefield separation.

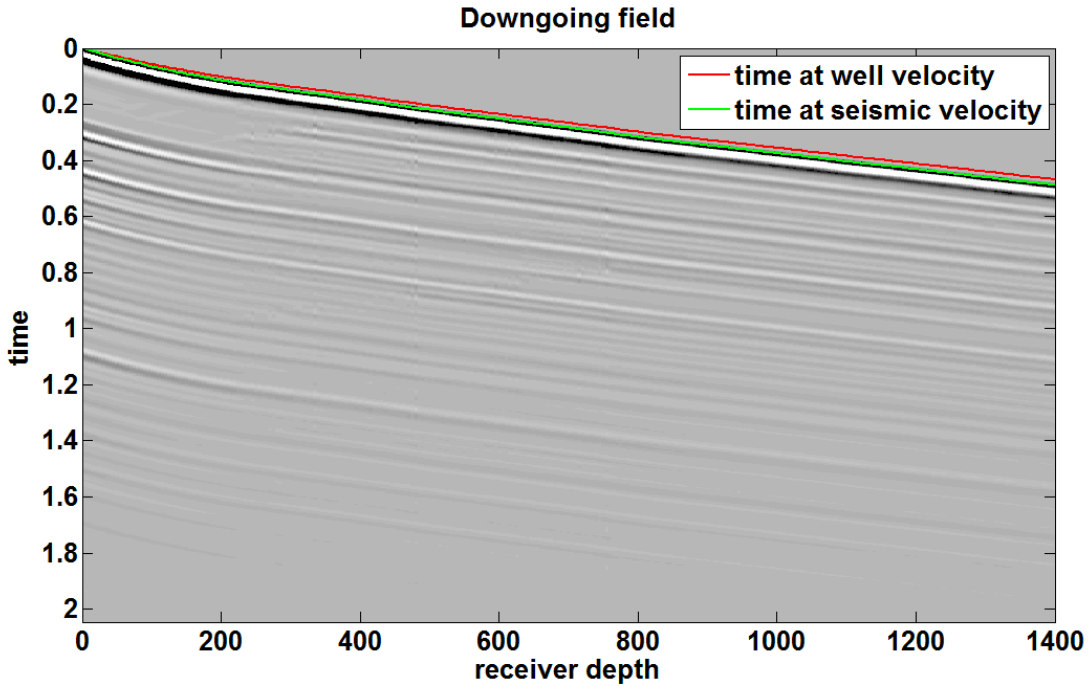

Figure 6: The downgoing wavefield from Figure 4. The sum of this and the upgoing field from Figure 5 gives the total field in Figure 4. Also shown are traveltime calculations showing that the first arrivals are later in time than predicted from the well velocities (see equation 2).

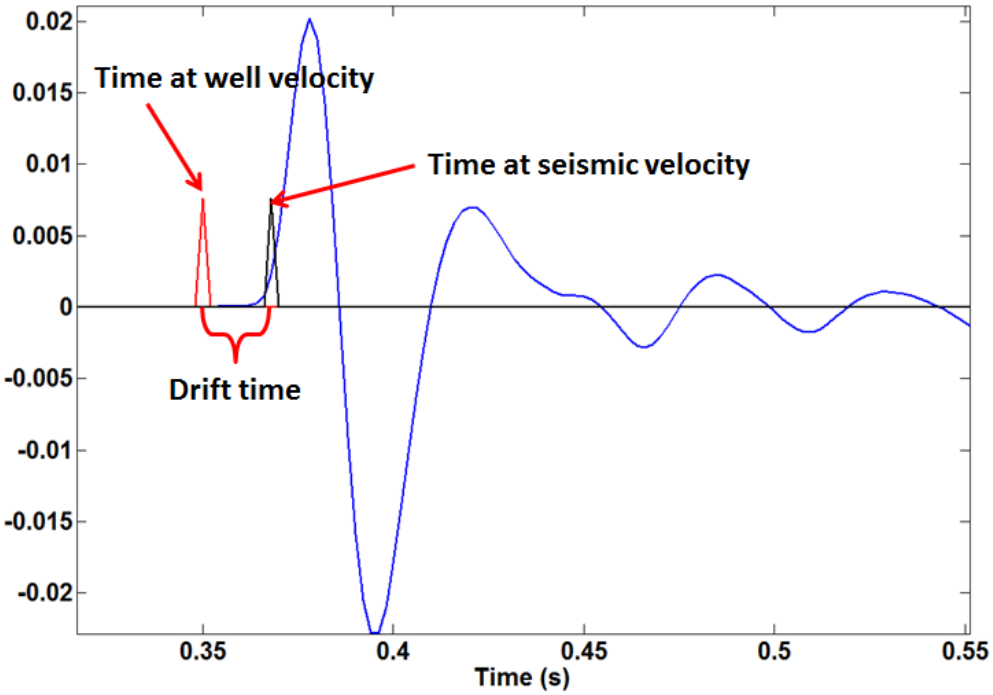

Figure 7: An enlargement of the downgoing wavefield at the deepest receiver of Figure 6. Also shown are traveltime computations at the well velocity and at the seismic velocity as determined by equation 2. The difference between these traveltimes, known as the drift, is an effect of attenuation theory and is accurately reproduced by the modelling algorithm.

The downgoing field of Figure 6 is suitable for Q measurements by the spectral-ratio method. The results of a set of measurements are shown in Figure 8. (In this, and all subsequent Q measurements in this paper, the downgoing traces were windowed with a 0.2s window that begins 0.02 s before the picked first arrival time. The window has no taper at the beginning but has a 20% raised cosine taper at the end. The measurements are not extremely sensitive to the window choice but this was used to ensure that only short delay multiples are allowed to contribute.) Examination of Figure 8 shows that the measured Q is consistently lower than the expected value, which will be called the Q bias. This is what would be expected if there is a second attenuation mechanism caused by the ODA stratigraphic filtering effect. However, there are other possible explanations including a possible systematic in the spectral-ratio calculation or an incorrect estimate of the transmission loss. Also, it would be appropriate to verify that the magnitude of the Q bias is what is expected from internal scattering.

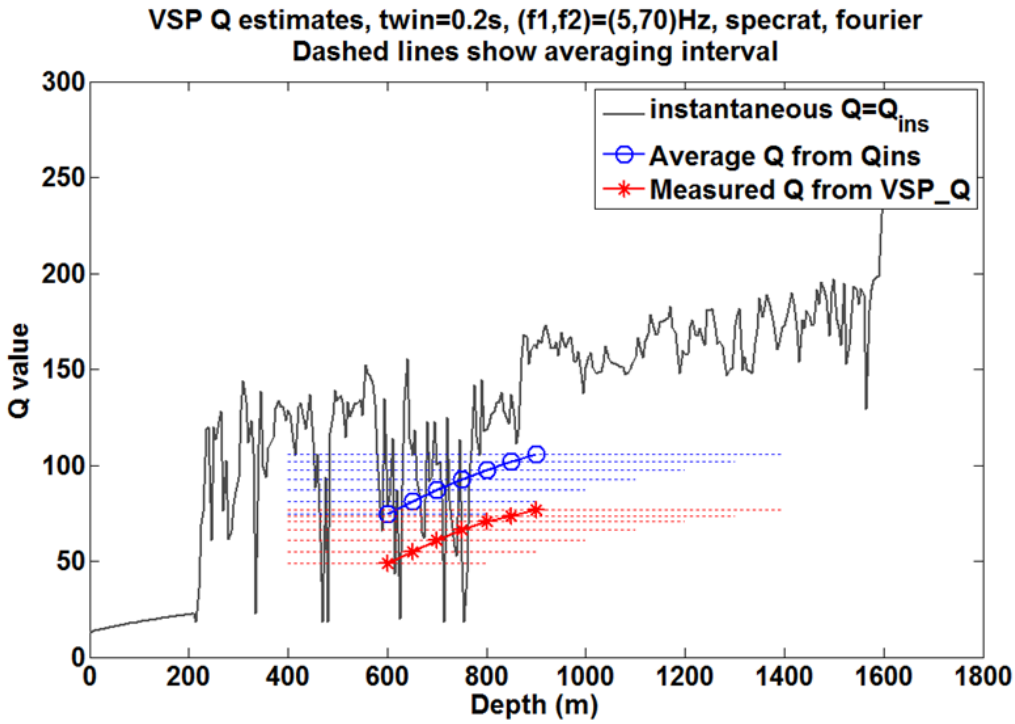

Figure 8: The result of 7 spectral-ratio computations on the downgoing wavefield of Figure 6. The black line is the Q curve used in the model of Figure 3. The red stars indicate the estimated Q values and each star has a horizontal dotted red line whose extent indicates the depth range represented by the measurement. The measurement was obtained by comparing a receiver at the depth of the beginning of the line to a receiver at the depth of the end of the line. Thus the 7 measurements all had the same shallow receiver and used progressively deeper receivers. The blue circles indicate the expected valued of the measurement as computed by equation 20.

The VSP modelling algorithm described previously can be run with a modified layer matrices that turn off internal multiples, transmission loss, or both. Figure 9 shows the downgoing wave that results when both internal multiples and transmission loss are turned off but still using the model of Figure 3. Spectral-ratio measurements made on this wavefield should have the greatest chance of success. Figure 10 shows the result of repeating the measurements of Figure 8 on the wavefield of Figure 9. As is apparent, there is excellent agreement between measurement and expectation, indicating that the spectral-ratio calculation is working reliably. Figure 11 shows a sample spectral ratio calculation (the deepest one) in which the *lsr* (equation 13) is very linear and the estimated transmission coefficient is essentially unity as we would expect.

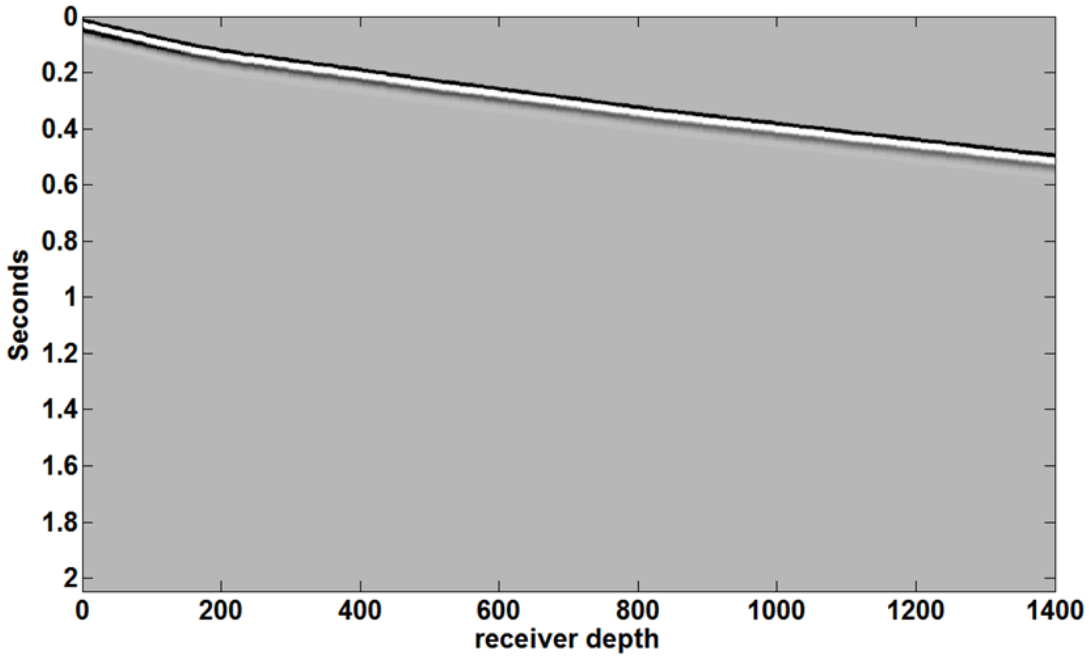

Figure 9: The downgoing wavefield that results when both transmission loss and internal multiples are turned off. Compare with Figure 6.

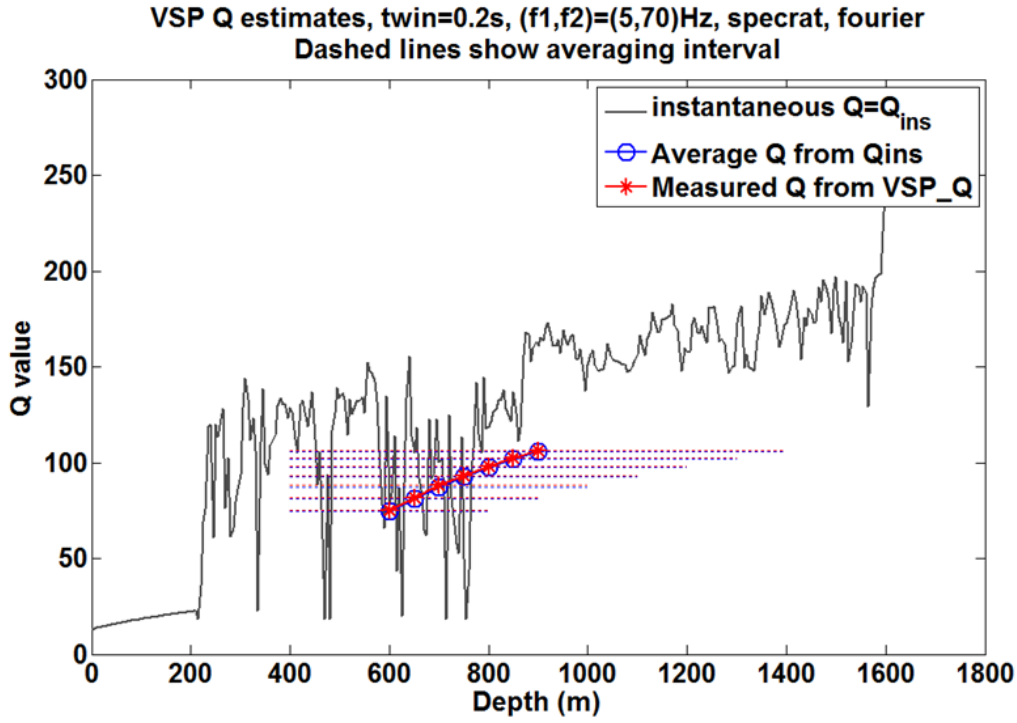

Figure 10: Similar to Figure 8 except that the spectral measurements were made on the wavefield of Figure 9 which has not internal multiples and not transmission loss.

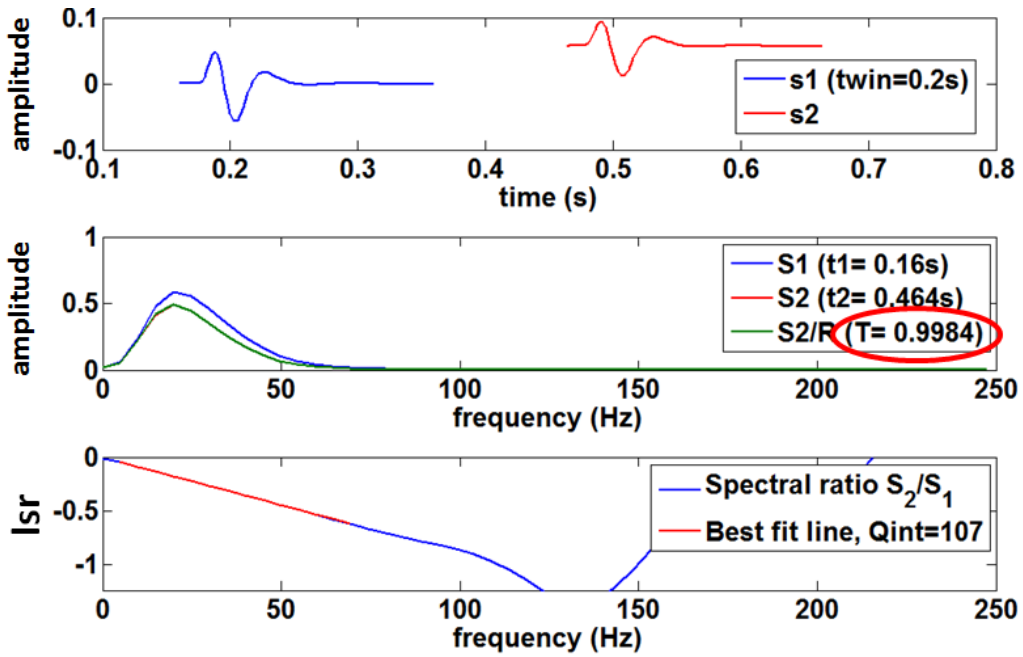

Figure 11: Illustration of a Sample spectral-ratio calculation from the results of Figure 10. The top axes shows the two time-domain waveforms that enter into the calculation. The middle axes shows the amplitude spectra of these waveforms and the estimated transmission coefficient is shown circled. The bottom axes shows the spectral ratio calculation with the lsr showing excellent linear behavior over a broad frequency range.

Next, we repeat these measurements with a downgoing field that includes transmission losses but still contains no internal multiples. This field, shown in Figure 12, looks almost identical to that in Figure 9 but careful examination shows that there is subtly greater decay in Figure 12. The resulting Q measurements, shown in Figure 13, again match the expectations computed from equation 20. The sample spectral-ratio calculation, shown in Figure 14, shows an *lsr* that is again very linear with the major difference being that the estimated transmission coefficient is reduced to about 0.62 .

Continuing in this fashion, the next three figures repeat these results with transmission losses and surface-related multiples but with internal multiples still turned off. Figure 15 is the downgoing field, Figure 16 the Q measurement results, and Figure 17 the sample spectral-ratio calculation. Again the result is a match between estimation and expectation and the *lsr* is very smooth and linear.

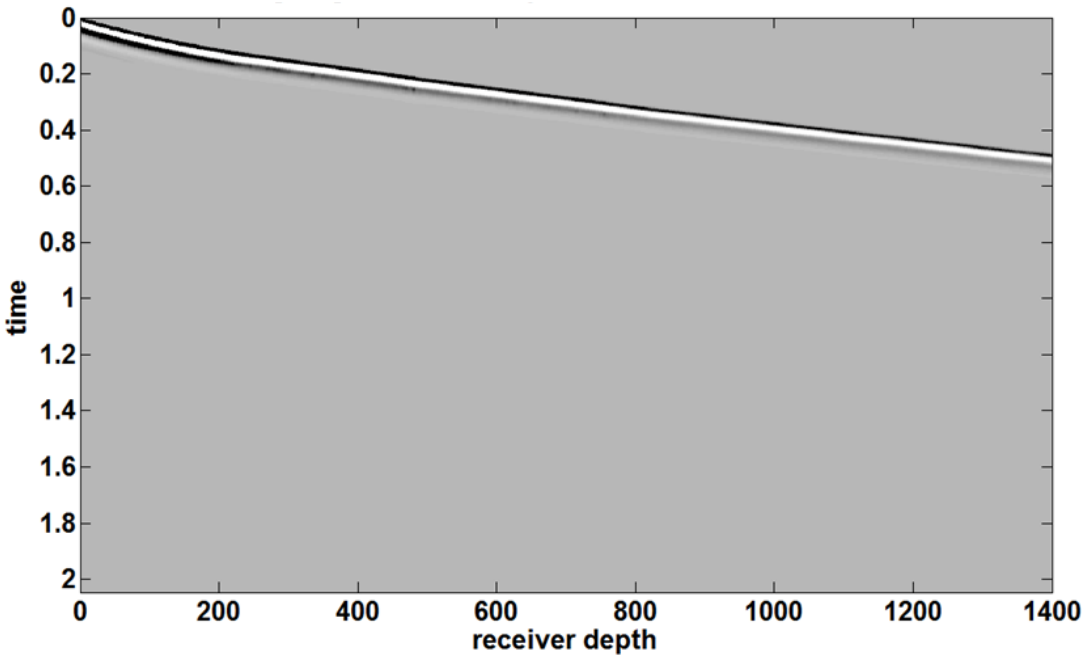

Figure 12: The downgoing field that results when transmission losses are included but internal multiples are not. Compare to the fields of Figures 6 and 9.

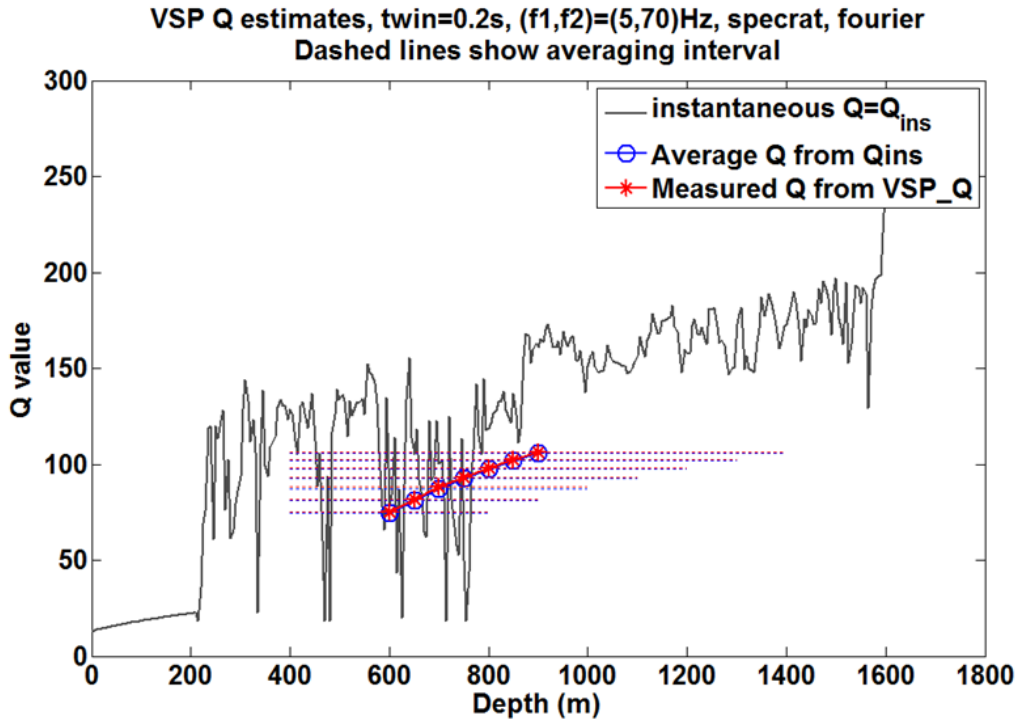

Figure 13: The result of spectral-ratio calculations on the wavefield of Figure 12. Again the result matches expectations. Compare with Figures 10 and 7.

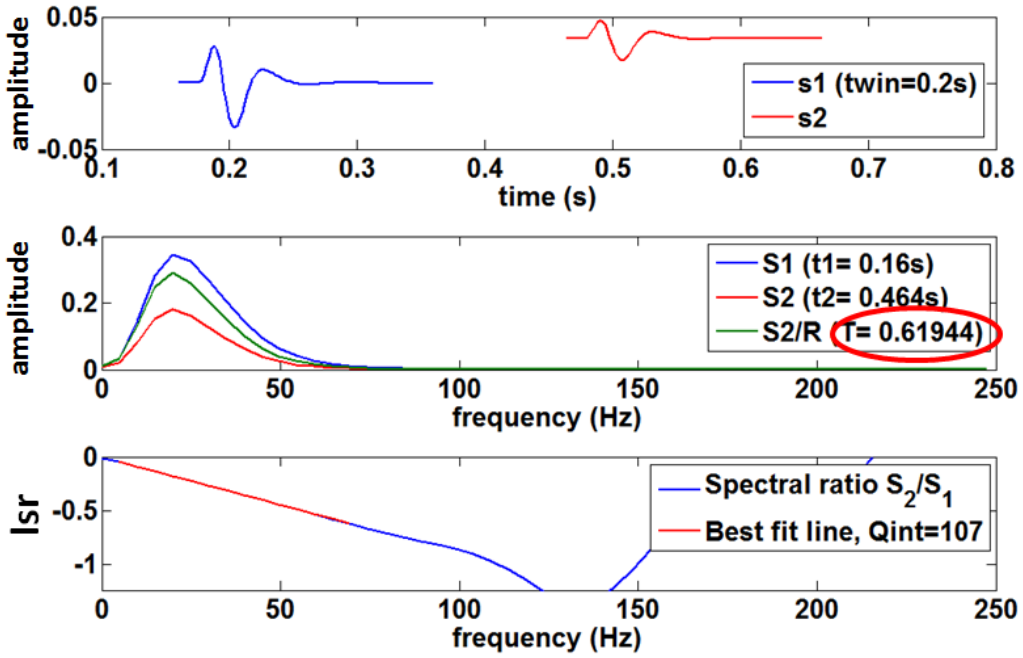

Figure 14: Example of a spectral-ratio calculation from the results in Figure 13. Compare with Figure 11. Note the estimated transmission coefficient is much smaller than in Figure 11.

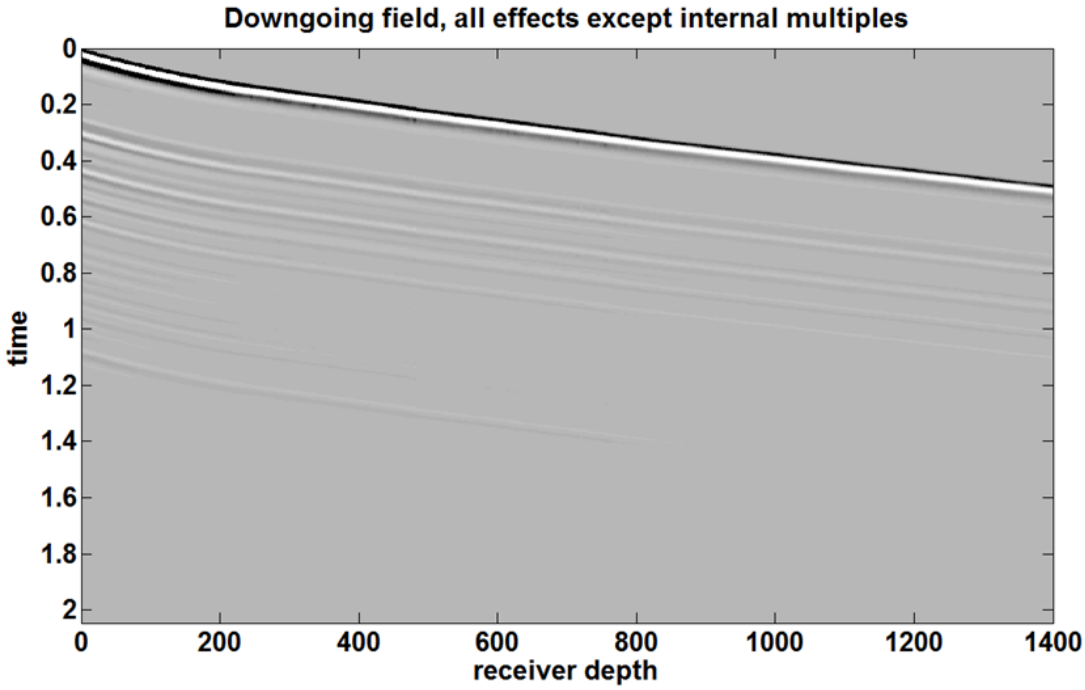

Figure 15: The downgoing field that results when all physical effect except internal multiples are turned on. That is, transmission effects and surface-related multiples are now present. Compare with Figures 12, 9, and 6.

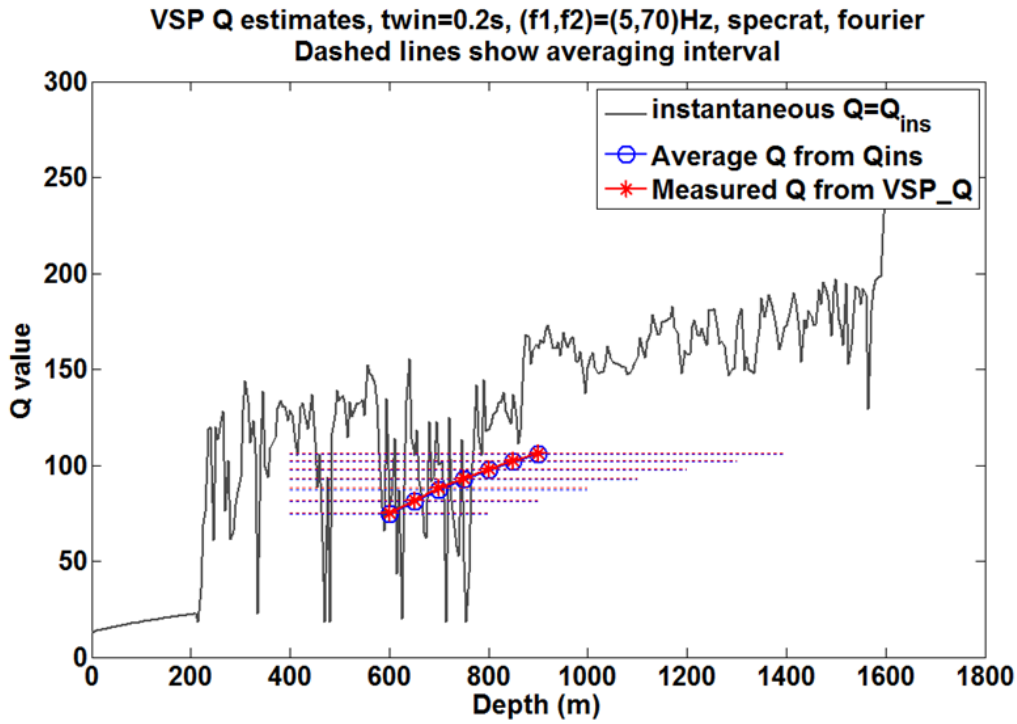

Figure 16: The result of spectral-ratio calculations on the wavefield of Figure 15. Again the result matches expectations. Compare with Figures 13, 10 and 7.

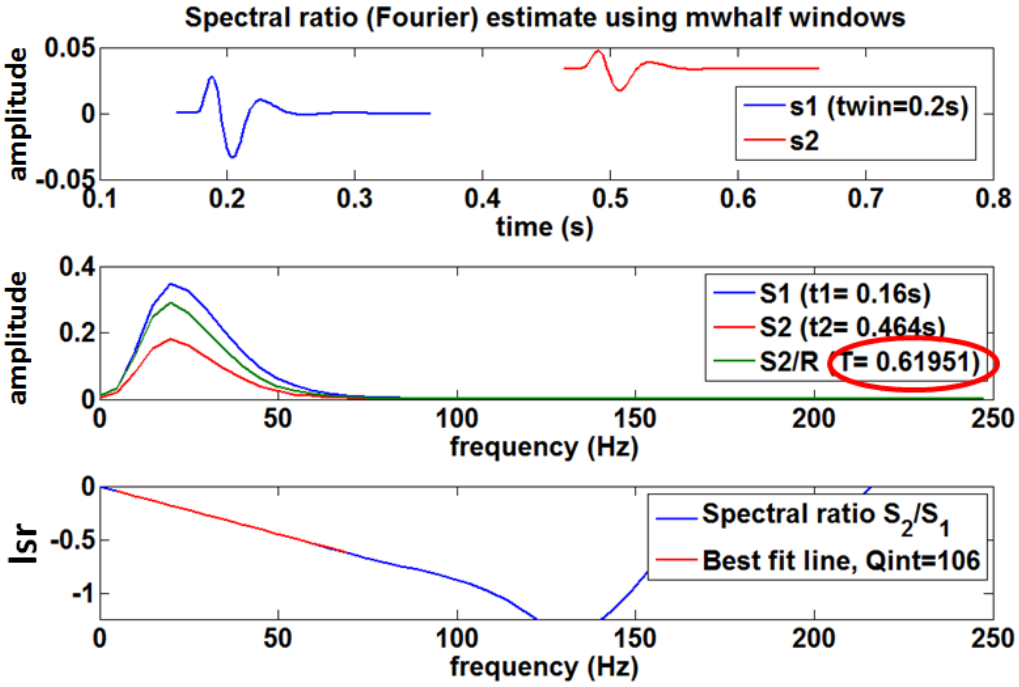

Figure 17: Example of a spectral-ratio calculation from the results in Figure 16. Compare with Figures 14 and 11. Note the estimated transmission coefficient is essentially the same as in Figure 14.

At this point, it has been verified that the spectral ratio measurements are working very accurately and give the expected result when all physical effects except for internal multiples are turned on. In figures 18, 19, and 20 is anther experiment in which internal multiples are now turned on, transmission losses are on, but surface-related multiples are off. The downgoing field shows a complex coda following the direct wave which has significant energy at all possible lags. In Figure 19 it is immediately apparent that the measurement bias has returned, confirming that internal multiples are the cause. In Figure 20, the example spectral-ratio calculation shows several features of interest. First the *lsr* is no longer smoothly linear but shows oscillations consistent with the complex interference pattern of the coda. Second, the transmission coefficient is estimated as larger than on measurements without internal multiples. This was predicated by ODA who showed that the low frequencies in the multiples reinforced the direct arrival while the high frequencies were attenuated. Figure 21, a reproduction of Figure 16 from O'Doherty and Anstey (1971), shows clearly their prediction of the reinforcing and pulse broadening effects of short-path internal multiples.

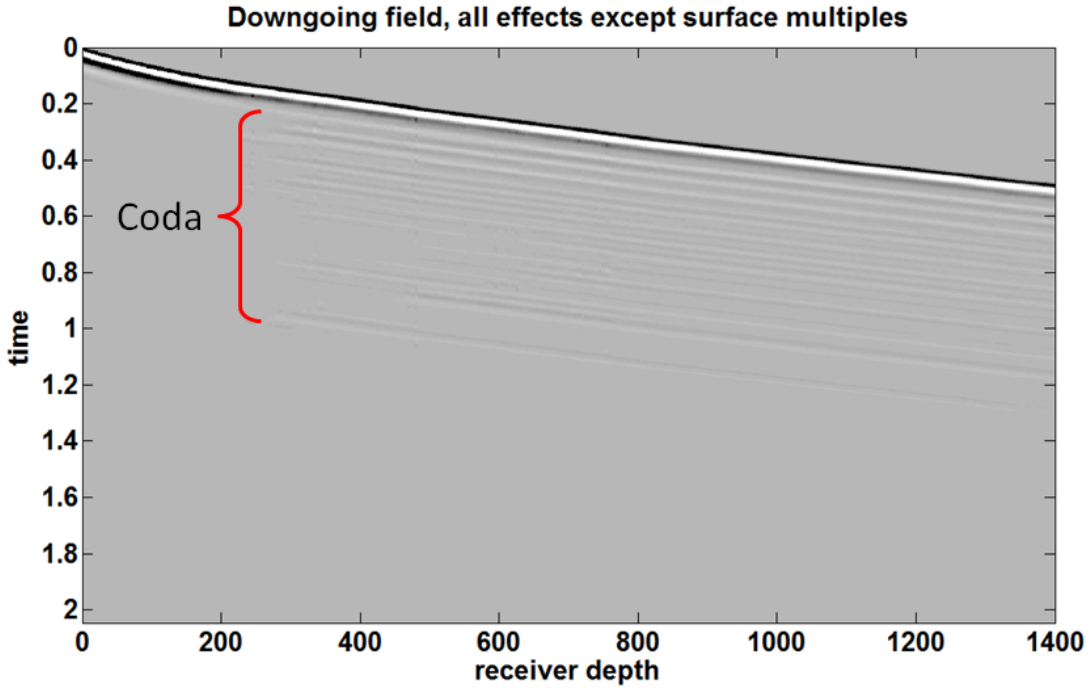

Figure 18: The downgoing field for the model of Figure 3 when all effects except surface-related multiples are turned on. The indicated coda is the result of internal multiples. Compare with Figures 15, 12, 9, and 6.

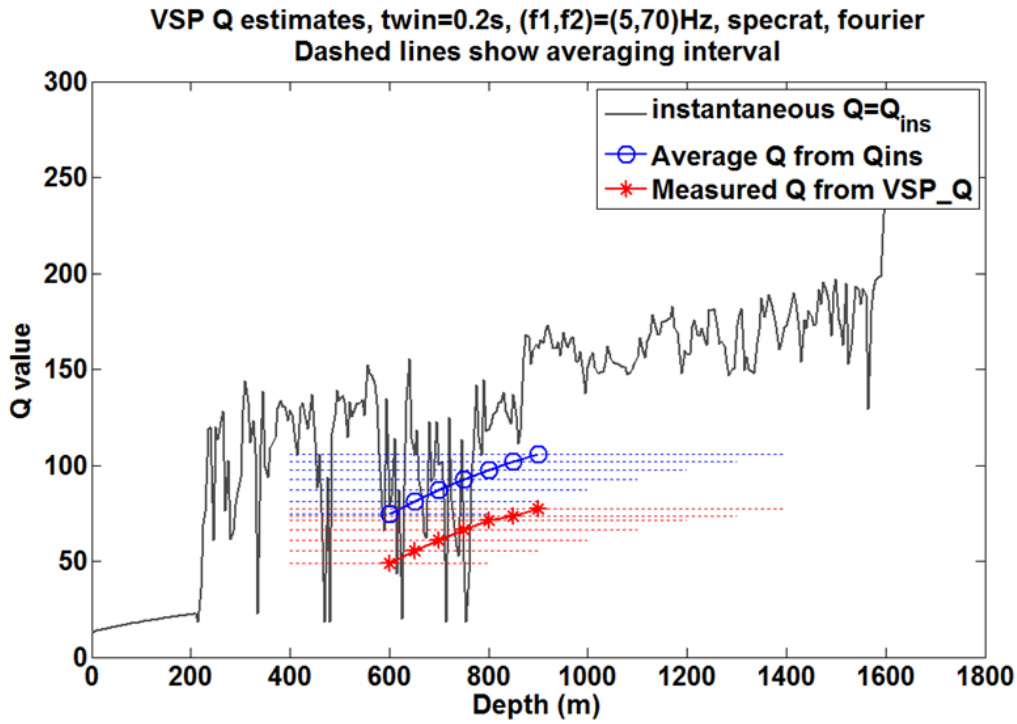

Figure 19: The result of spectral-ratio measurements on the downgoing field of Figure 18. Compare with Figures 16, 13, 10, and 8. Here the measurement (red stars) disagrees with the expectation (blue circles) confirming that internal multiples are causing the bias.

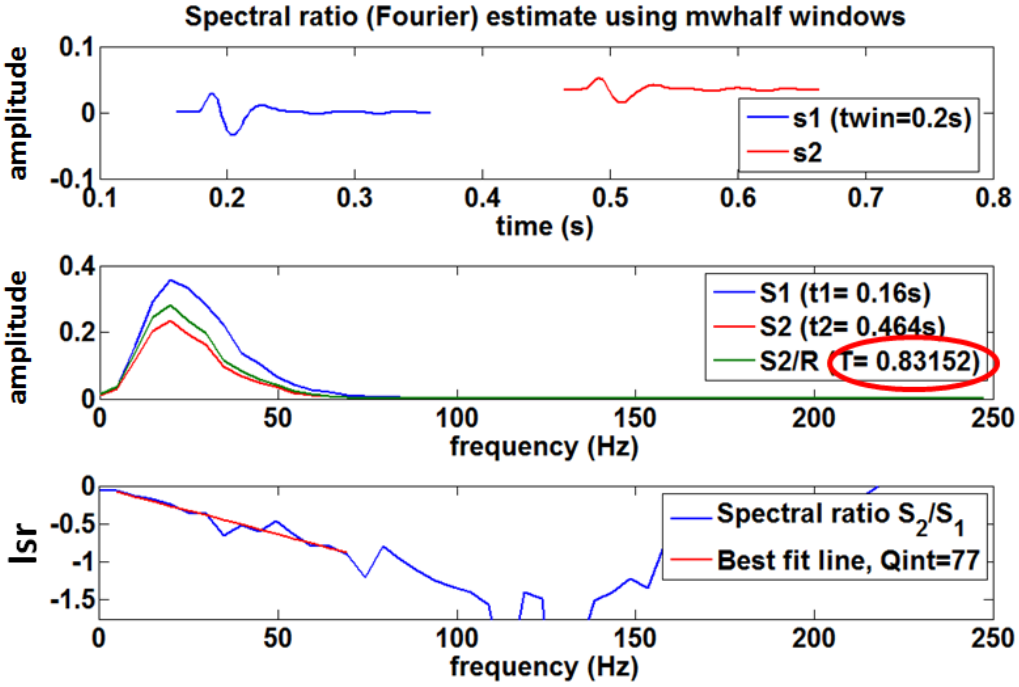

Figure 20: Example of a spectral-ratio calculation from the results in Figure 19. Compare with Figures 17, 14 and 11. Note the estimated transmission coefficient is larger than that in Figure 14.

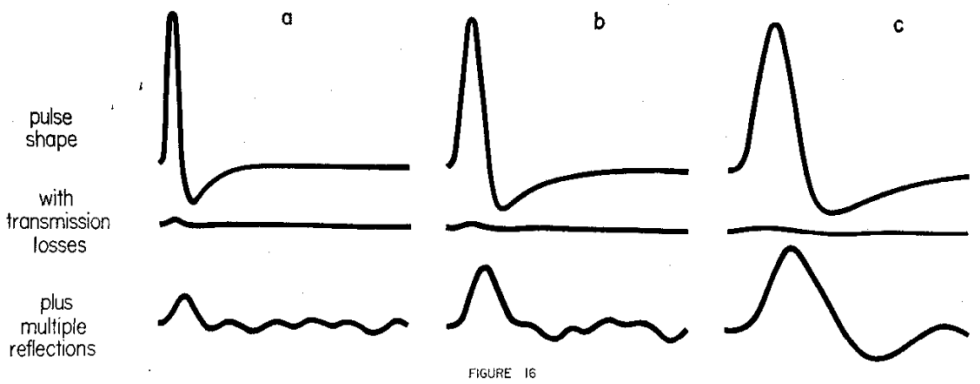

Fig. 16. The effect of convolving three seismic pulse shapes with the pulse formed by transmission through the log of fig. 12, without and with the effect of the very-short-delay multiple reflections.

Figure 21: A reproduction of Figure 16 from O'Doherty and Anstey (1971).

As a further confirmation, the VSP was recalculated with $Q = \infty$ in all layers which turns off intrinsic attenuation. Spectral-ratio measurements still give significant Q values shown as the red stars in Figure 22. These are direct measurements of the stratigraphic quality factor Q_{strat}. It should then be the case that the intrinsic quality factor, $Q_{\text{intrinsic}}$ (the blue circles in Figure 22), and the effective quality factor, Q_{eff}, should relate to Q_{strat} via (Richards and Menke, 1983)

$$\frac{1}{Q_{\text{eff}}} = \frac{1}{Q_{\text{intrinsic}}} + \frac{1}{Q_{\text{strat}}}. \tag{21}$$

The Q measurements in Figure 19 are measurements of Q_{eff}. Figure 23 shows the result of this computation and confirms that the direct measurements of Q_{eff} and Q_{strat} are consistent with the intrinsic $Q_{\text{intrinsic}}$.

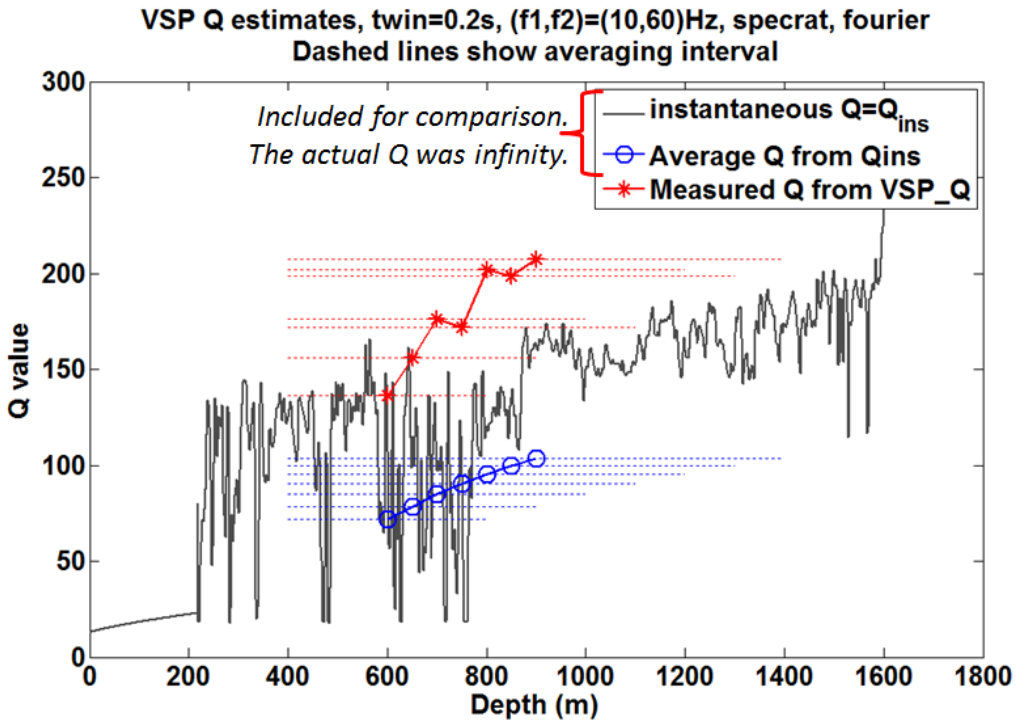

Figure 22: The Q measurements resulting from a re-computed VSP in which $Q = \infty$ was prescribed in all layers. The measured values are the red stars while the black curve showing the intrinsic Q and the blue ovals are the same as in previous figures and are included for comparison.

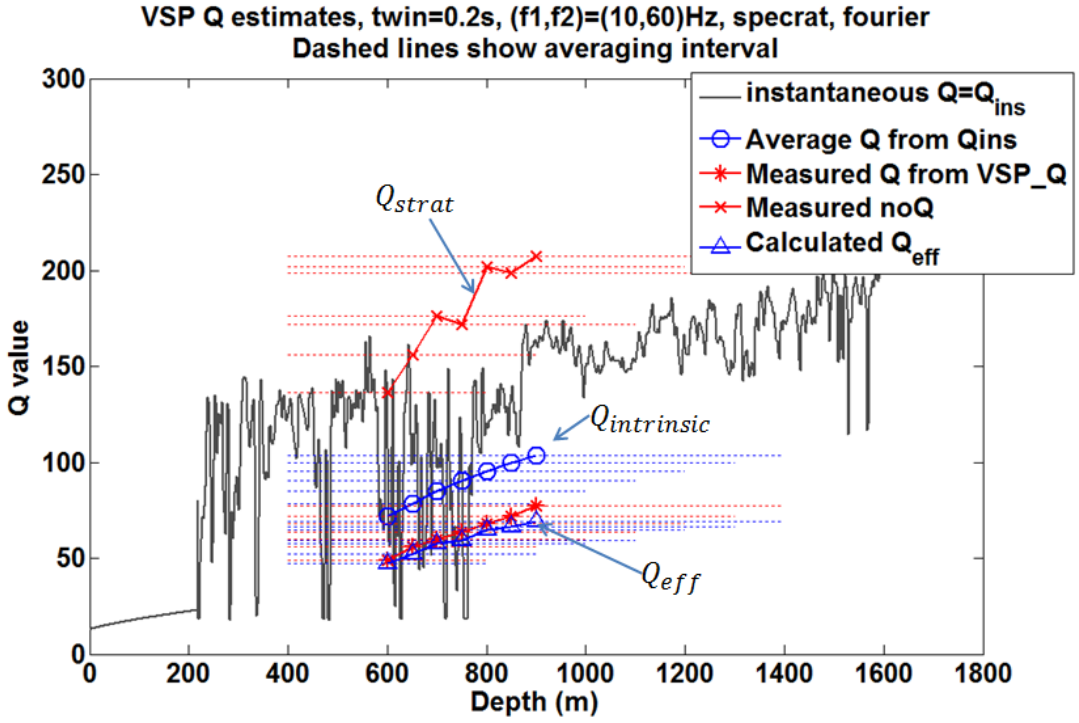

Figure 23: The result of combining Q_{strat} and with equation 21 gives Q_{eff} which is essentially equal to the measured Q in Figure 19.

Having established that the VSP modelling algorithm shows stratigraphic filtering as predicted by ODA and which is completely consistent with constant Q theory, a further "blocking study" experiment reveals just how "fine" a finely layered model must be to show this effect. A series of geological models were created from the logs in Figure 3 with progressively coarsening blocking sizes over the range 0.5m to 80m. For each model, Backus averages of velocity and density were calculated over the blocking size although all models were sampled at the same 0.5m. Therefore, each model had the same number of computational layers (one every 0.5m) but the number of physical layers was determined by the blocking size. For each model the VSP response was computed and spectral-ratio measurements were made on the downgoing fields for a set of intervals. Figure 24 shows 6 selected results from this analysis using the same figure format as, for example, Figure 19. It is apparent that stratigraphic filtering vanishes for blocking sizes greater than about 10m. Also displayed on each panel of this figure is the wavelet used in the simulations (it was the same for each simulation) and it can be seen that the dominant wavelength is about 100m. So the blocking size at which stratigraphic filtering vanishes is about 10% of the dominant wavelength.

Another way to analyze this blocking study is to calculate the Q_{bias} defined by

$$Q_{\text{bias}} = \bar{Q}_{\text{intrinsic}} - \bar{Q}_{\text{eff}} \tag{22}$$

where the overbar indicates the average value. Thus, the Q_{bias} is the average value of the expected result minus the average value of the measured result. When stratigraphic filtering is present, Q_{bias} should be positive. Figure 25 plots Q_{bias} versus blocking size for each model used in the study. As can be seen, stratigraphic filtering is a strong effect for blocking sizes less than 5m. Given that the sample interval of the logs used was 1ft, it is not possible to explore Q_{bias} for significantly smaller blocking sizes that the minimum used here which was ½m. However, while it seems likely that the fine layering of the earth knows no natural lower bound, it is not clear that finer structured models would produce a larger Q_{bias}. What is especially interesting about Figure 25 is that it indicates that the stratigraphic filtering effect effectively vanishes for blocking sizes greater than about 10m and Q_{bias} first becomes negative for a blocking size of 20m. Both of these numbers are much less than the 100m dominant wavelength of the wavelet used in this study. This dominant wavelength was computed from the dominant frequency of 30Hz using a mean velocity of 3000m/s. The spectral-ratio analysis was done over a frequency band of 10-60 Hz so that the wavelength at the highest analysis frequency is estimated at 50m, still much larger than the 10m blocking size where Q_{bias} becomes negligible. So, it seems that the fineness of the layering required to see stratigraphic filtering in the seismic band is of the same order as the 1ft sample size in common well logs. Blocking the logs to 2m, a 6-to-1 downsampling should still show the effect but one should be cautious about any greater blocking.

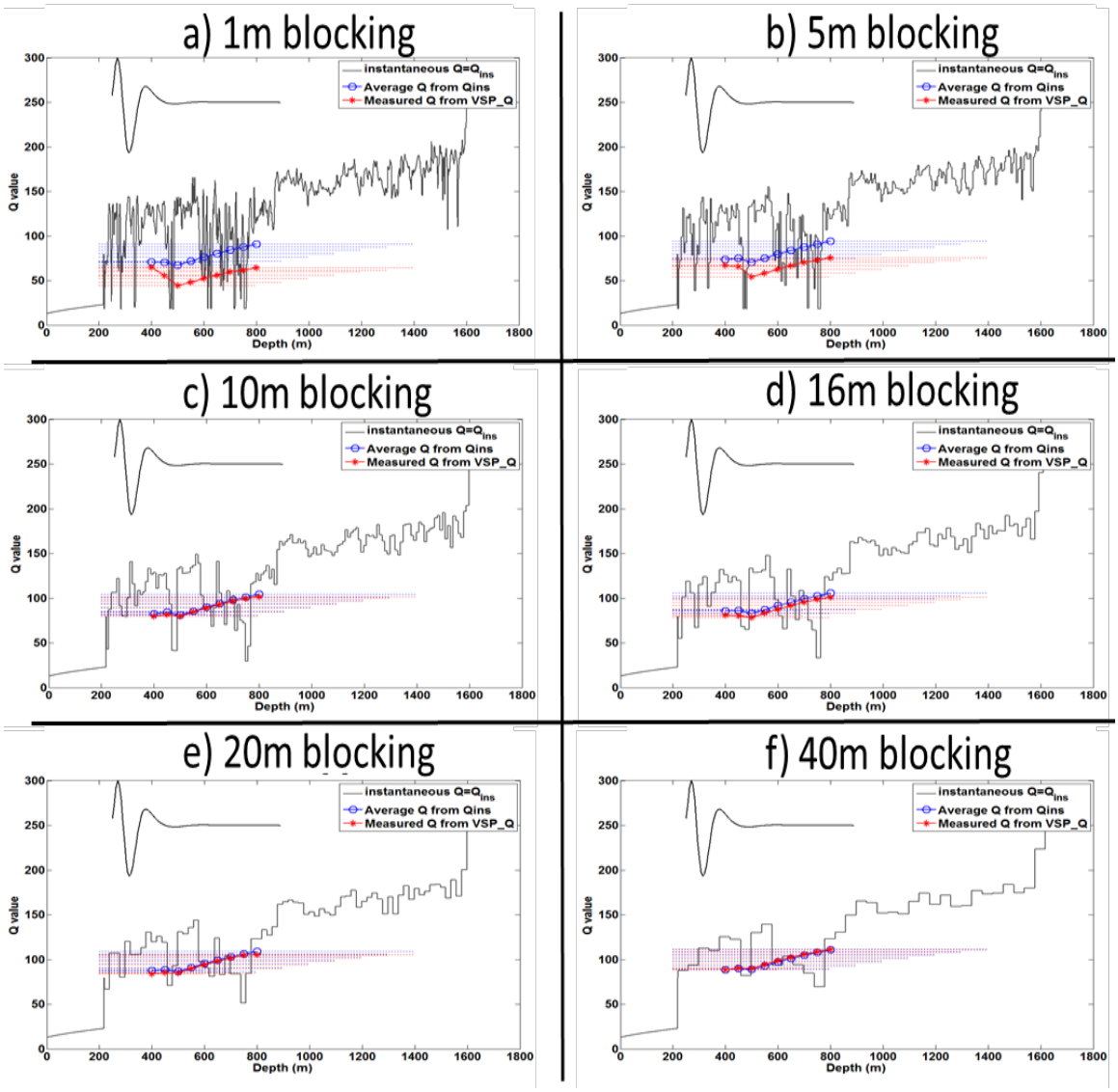

Figure 24: A sequence of results in which the blocking size of the model was progressively increased. In each case, the model was derived from the logs shown in Figure 3 but with the blocking (or averaging) size as shown. The model was sampled at 0.5m in each case. The panels show the blocked $Q_{\text{intrinsic}}$ as a black line and the spectral-ratio estimates are red stars while the expected results are the blue ovals. Each panel also shows the wavelet used in the seismic modelling in correct relative scale. There is very little evidence of stratigraphic filtering after a blocking size of 10m and it vanishes altogether above 20m.

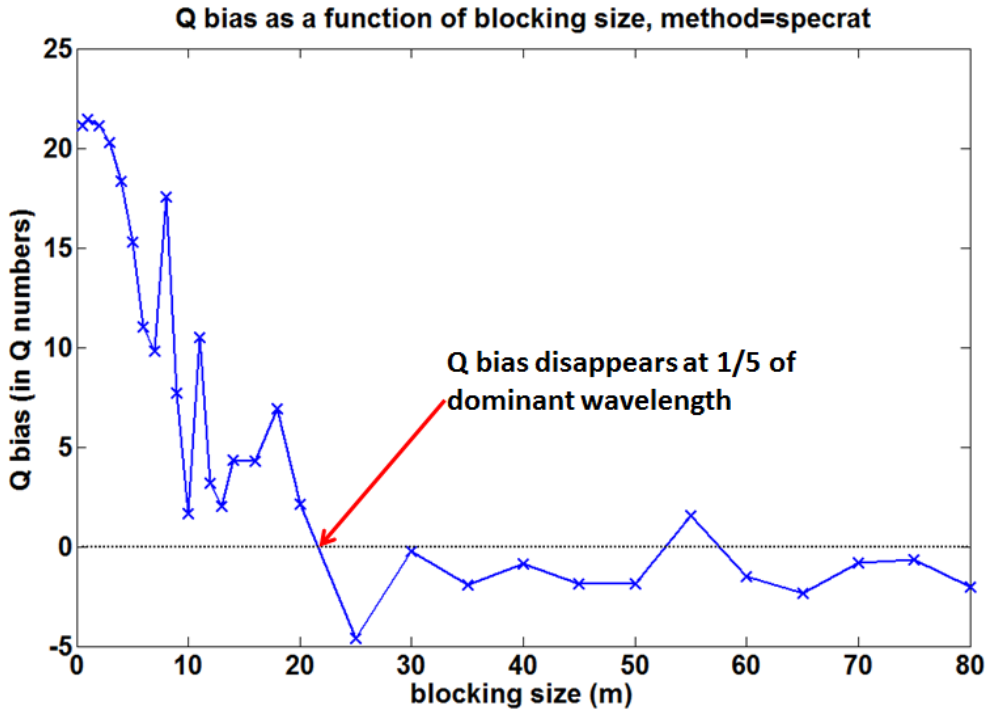

Figure 25: The Q_{bias} (defined by equation 22) as calculated from the blocking study described in the text and also as displayed in Figure 24. The dominant wavelength of the wavelet used in the study was 100m and Q_{bias} first becomes negative at a blocking size of 20m which is 1/5 of the dominant wavelength. It is likely that the Q_{bias} is negligible for blocking sizes greater than 10m.

CONCLUSIONS

A new 1D VSP modelling code, which includes the effects of Q attenuation, has been demonstrated to accurately model the apparent attenuation produced by fine layering. The modelling code is both efficient and accurate, being able to model thousands of layers in about 1 minute or less. The code models all multiples, transmission losses, and Q effects. To demonstrate stratigraphic filtering, a model with some 3500 layers was created from well log information. Each layer was 0.5m thick and velocity and density values were prescribed from well logs. A Q value, called $Q_{\text{intrinsic}}$, was prescribed for each layer using an empirical relation between Q and velocity and density. The downgoing wavefield from the synthetic VSP predicted from this model was then measured for Q values using spectral ratios. The expected value of Q from these measurements is than predicted from appropriate averages of the known $Q_{\text{intrinsic}}$ profile. It was found that the measured Q was always less than the expected value by a significant amount. Experimentation showed that when internal multiples were turned off in the modelling that the measured and expected values agreed. Thus the internal multiples are biasing Q measurements to lower values. This was predicted over 40 years ago by O'Doherty and Anstey (1971) and has been called stratigraphic filtering since then. While the original O'Doherty and Anstey paper addressed the emergence of stratigraphic filtering from finely layered elastic media, this numerical study has

demonstrated the extension to attenuating acoustic media. The stratigraphic filtering Q, called Q_{strat} can be measured directly by setting $Q_{\text{intrinsic}} = \infty$ in all layers and repeating the modelling and spectra ratio measurements. These numerical estimates are in close agreement with the relation $Q_{\text{eff}}^{-1} = Q_{\text{intrinsic}}^{-1} + Q_{\text{strat}}^{-1}$ where Q_{eff} is the effective Q measured in finely-layered attenuating media. A further series of experiments were conducted in which the layer thicknesses were varied from 0.5m to 80m, in each case computing the layer properties from Backus averages from the same well logs. Comparison of the measured Q_{eff} with the prescribed $Q_{\text{intrinsic}}$ shows that stratigraphic filtering really only become obvious and measurable for layer thicknesses less than 10m. Thus, the question "How fine is finely layered?" has the answer "Less than 10m.".

ACKNOWLEDGEMENTS

I thank the sponsors of CREWES for their support. I also gratefully acknowledge support from NSERC (Natural Science and Engineering Research Council of Canada) via two grants: CRDPJ 379744-08 and RGPIN 217032-2013.

REFERENCES

Backus, G., 1962, Long-wave elastic anisotropy produced by horizontal layering: Journal of Geophysical Research, 67, no. 11, 4427-4440.

Banik, N. C., I Lerche, and R. T. Shuey, 1985, Stratigraphic filtering, Part 1: Derivation of the O'Doherty-Anstey formula, Geophysics, 50, 2768-2774.

Bath, M., 1974, Spectral analysis in geophysics: Developments in Solid Earth Geophysics, Vol 7, Elsevier Science Publishing Co.

Berlyand, L., and Burridge, R., 1995, The accuracy of the O'Doherty-Anstey approximation for wave propagation in highly disordered stratified media: Wave Motion, 21, 357–373.

Cheng, P., 2013, Anelastic attenuation in seismic data: modelling, measurement, and correction: PhD thesis, University of Calgary.

Ganley, D. C., 1981, A method for calculating synthetic seismograms which include the effects of absorption and dispersion, GEOPHYSICS Aug 1981, Vol. 46, No. 8, pp. 1100-1107.

Kjartansson, E, 1979, Constant Q-wave Propagation and Attenuation, Journal of Geophysical Research, 84, 4737-4748.

Liner, C. L., 2012, Elements of Seismic Dispersion, A Somewhat Practical Guide to Frequency-dependent Phenomena, Society of Exploration Geophysicists, Distinguished Instructor Series, No. 15.

O'Doherty, R. F., and N. A. Anstey, 1971, Reflections on Amplitudes, Geophysical Prospecting, 19, pp. 430-458.

Richards, P. G., and W. Menke, 1983, The apparent attenuation of a scattering medium: Bulletin of the Seismological Society of America, 73, 1005-1021.

Schoenberger, M., and F. K. Levin, 1974, Apparent attenuation due to interbed multiples: Geophysics, 39, 278-291.

Tonn, R., 1991, The determination of seismic quality factor from VSP data: A comparison of different computational methods: Geophys. Prosp., 39, 1-27.